



CHALMERS
UNIVERSITY OF TECHNOLOGY

Softening Behavior of a Cold Work Tool Steel and High-Boron Tool Steel Fabricated by Directed Energy Deposition

Downloaded from: <https://research.chalmers.se>, 2024-03-13 06:55 UTC

Citation for the original published paper (version of record):

Yuan, M., Nyborg, L., Oikonomou, C. et al (2023). Softening Behavior of a Cold Work Tool Steel and High-Boron Tool Steel Fabricated by Directed Energy Deposition. Steel Research International, In Press. <http://dx.doi.org/10.1002/srin.202300192>

N.B. When citing this work, cite the original published paper.

Softening Behavior of a Cold Work Tool Steel and High-Boron Tool Steel Fabricated by Directed Energy Deposition

Miwen Yuan, Lars Nyborg, Christos Oikonomou, Seshendra Karamchedu, Yicheng Fan, Libin Liu, and Yu Cao*

Prolonging the life of hot stamping dies in the automotive industry is challenging. Surface modification is an effective way to improve the durability of the dies. In this study, two tool steel grades, one cold work tool steel (V4E) and one high-boron tool steel (HBS), are deposited on a tool steel substrate using directed energy deposition, followed by tempering. Softening behavior at high temperatures of 550 and 600 °C is investigated. In the key findings, it is revealed that both steels exhibit remarkable hardness, surpassing the substrate even after extended exposure to high temperatures. HBS shows excellent softening resistance in terms of hardness at 550 °C but experiences a significant drop at 600 °C. V4E demonstrates an overall superior softening resistance due to its thermal stable MC (M represents metal) carbides and the relatively stable dislocation density. Microstructural analysis highlights some unique features, such as borides in HBS and dendritic structures in V4E. In this study, the correlation between microstructure characteristics and hardness evolution is revealed, providing some insights into how these materials resist softening to enhance the longevity and performance of hot stamping dies.

nozzle are moved coaxially in the process of DED. This method can deposit metal powder on the surface with any shape, providing a great advantage in workpiece repair and hardfacing^[3,4] to increase the hardness and wear resistance.

Certainly, alternative methods exist for the repair and hardfacing of tools. For example, physical vapor deposition offers the capability to apply protective layers onto the die surface, resulting in a substantial enhancement of surface hardness and wear resistance,^[5,6] but the compatibility between these coatings and the substrate remains a concern, as prolonged exposure to wear, cyclic heating, and cooling during the hot stamping process may lead to erosion and detachment. Other material modification approach, such as increasing hardness through nitriding, can aid in enhancing the resistance to abrasion. However, nitriding may also introduce the risk of fatigue fracture occurring in


the surface-proximate regions of the tool.^[7] Nevertheless, the DED method can achieve a good bonding between the coating layer and the substrate and is promising to improve the wear resistance of tools.

High-temperature resistance against softening is a critical property for the tool steels applied in hot stamping. There are two main approaches to improving the high-temperature resistance of hot work tool steel. The first one is the proper design of the chemical composition of the steel. The principle is to

1. Introduction

Additive manufacturing is a method that can produce near-net shapes and has the ability to reduce process steps in manufacturing.^[1,2] It has found wide applications in aerospace and automobile industry. Directed energy deposition (DED) is an additive manufacturing method that uses a laser as a heat source to melt metal powders and deposit the materials onto an existing substrate material. Generally, the laser and powder feeding

M. Yuan, L. Nyborg, Y. Cao
Department of Industrial and Materials Science
Chalmers University of Technology
41296 Gothenburg, Sweden
E-mail: yu.cao@chalmers.se

 The ORCID identification number(s) for the author(s) of this article can be found under <https://doi.org/10.1002/srin.202300192>.

© 2023 The Authors. Steel Research International published by Wiley-VCH GmbH. This is an open access article under the terms of the Creative Commons Attribution-NonCommercial-NoDerivs License, which permits use and distribution in any medium, provided the original work is properly cited, the use is non-commercial and no modifications or adaptations are made.

DOI: 10.1002/srin.202300192

M. Yuan, L. Liu
School of Materials Science and Engineering
Central South University
Changsha 410083, P. R. China

C. Oikonomou, S. Karamchedu
Research and Development Department
Uddeholms AB
Hagfors 638 85, Sweden

Y. Fan
Laser Cladding Department
ASSAB Tooling Technology (Shanghai) Co., Ltd.
Shanghai 201108, P. R. China

minimize the formation of primary carbides during the solidification and therefore maximize the precipitation of secondary carbides under the premise of high alloy composition.^[8] This is because in general the primary carbides have a large size, and their distribution is not uniform. In contrast, the secondary carbides are often finer and more uniform, which is beneficial to the material strength without the loss of ductility. Furthermore, if the secondary carbides are difficult to grow and coarsen, the softening resistance of the steels can then be improved at high temperatures due to the Zener effect. The second approach is the selection of manufacturing methods and suitable heat treatment. One of the main application areas of DED is hardfacing for molds made of tool steel. Compared with casting and welding, the cooling rate in a DED process is much faster, which can inhibit the back diffusion of alloying elements in solid.^[9] Consequently, more alloying elements can be trapped in the matrix with reduced macrosegregation. These trapped alloy elements can strengthen the material in the form of fine precipitates with appropriate post-heat treatments, thereby increasing the strength of the material at high temperatures.

The high susceptibility of tool steel to cracking (both hot and cold cracking) leads to poor processability of DED. There has been a lot of effort to improve the quality of the deposited parts. Park et al.^[10] investigated the influence of energy input on H13 and D2 tool steels and reported that this parameter can affect the layer height, microstructure, and carbon content of the deposited material. However, the hardness of the deposited H13 steel is higher than that of wrought H13 steel regardless of energy input, whereas this is not the case for D2 steel. This indicated that whether the hardness of the deposited steel is higher than that of the wrought steel or not is material dependent. Rahman et al.^[11] successfully deposited two types of high-speed steel with high carbon contents (>2 wt%) by means of preheating at 150 °C. The tensile tests showed both deposited steel grades fractured in a brittle failure manner, although high hardness had been achieved. Jeong et al.^[12] added a buffer layer of P21 steel between the deposited high-carbon tool steel (M2) and substrate to increase the processability. The study confirmed that this buffer layer could improve strength and toughness. High hardness and wear resistance could be achieved by the M2 hardfacing layer.

Most studies in literature focus on the characterization of the microstructure and properties of tool steels in either as-deposited or post-heat-treated conditions. Few studies focus on the softening resistance of the deposited materials at high temperatures. In the present study, a cold work tool steel (Uddeholm Vanadis 4 Extra SuperClean, hereafter denoted as V4E) and a newly developed high-boron tool steel (HBS) were deposited on a tool steel substrate. Appropriate post-heat treatments were applied and long-term softening resistance was evaluated. The purpose of this work is to assess the softening behavior of the hardfacing materials at high temperatures, as the dies in the hot stamping process operate at temperatures from room temperature up to 600 °C. In addition, the softening mechanisms of different tool steels are compared and discussed. The purpose of this study is to provide insights into the softening resistance of these tool steels at high temperatures, to improve the durability and performance of hot stamping dies in automotive manufacturing.

2. Experimental Section

To enhance the wear resistance of the tools, two Uddeholm tool steel grades, V4E (see Table 1), a cold work tool steel, and HBS, a high boron-containing tool steel (X50MoCoCr17-4), were deposited on the substrate. The powder employed in this investigation underwent sieving with the particle size range of 45–150 µm, resulting in D10, D50, and D90 values of 52, 73, and 125 µm, respectively. The Hall flow rate measured was 15 s, and the apparent density of the powder was determined to be 4.4 g cm⁻³. The substrate material used was Dievar with bulk dimensions of 117 × 59 × 25 mm³. Surface deposition was executed using a 5-axis DED laser machine equipped with a 4000 W laser source. The coaxial powder feeding nozzles maintained a focal distance of 16 mm. Argon gas was employed as the shielding gas, with a flow rate of 18 L min⁻¹. The 4-layer depositions were conducted in two areas of 52 × 52 mm (Figure 1). Each individual layer had a thickness of 1.6 mm.

To obtain the desired hardness, tempering is usually needed to form tempered martensite and remove the retained austenite (RA). Tempering parameters were optimized to obtain the highest hardness. The parameters determined were 2 h for three times at 550 °C for V4E and 2 h for two times at 525 °C for HBS, respectively. Regarding the application in hot stamping, it was critical to evaluate the softening resistance at elevated temperatures. Hence, after the tempering, the samples were subjected to time-dependent softening treatments at 550 and 600 °C for 5, 25, 50, and 100 h followed by air cooling to room temperature. Subsequently, hardness measurement was conducted on the samples.

Cubic samples with a size of 10 × 10 × 10 mm were extracted from the deposited bricks and then ground until 2000 SiC grit paper, followed by mechanical polishing using 1 µm diamond suspension and etching with a solution of 5% picric acid +1% HCl +94% ethanol for 15 s. Carl Zeiss Axioscope 7 was applied to take optical images which were then stitched together

Table 1. Chemical composition of the substrate and deposited powders (wt%).

	C	Si	Mn	Cr	Mo	V	Fe
Substrate	0.35	0.2	0.5	5.0	2.3	0.6	Bal.
V4E	1.4	0.4	0.4	4.7	3.5	3.7	Bal.

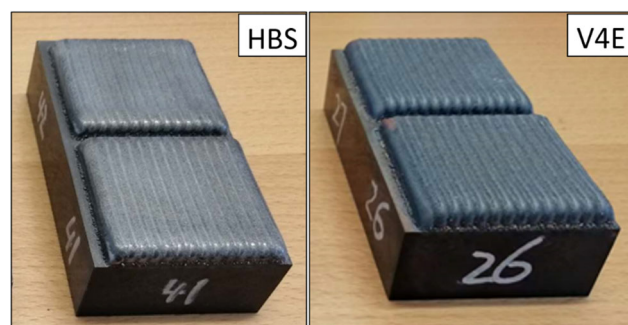


Figure 1. Laser-deposited V4E and HBS bricks.

to obtain an overall image of the sample. LEO/ZEISS Gemini 1550 scanning electron microscope (SEM) was used to observe the microstructure evolution and collect the backscattered images. The used voltage is 10 KV and the work distance is about 10 mm. X-ray diffraction (XRD) was used to inspect the phase constitution in the polished samples by means of a Bruker D8 Discover instrument with Cu-K α radiation ($\lambda = 1.54 \text{ \AA}$) operated at 40 Kv and 40 mA. The scanning speed was 1 s step^{-1} and the step size was $0.03^\circ \text{ step}^{-1}$. The detailed microstructure was further characterized by a transmission electron microscope (TEM, FEI Tecnai T20 LaB6) operated at 200 KV. TEM foil samples were finely ground to a thickness of $80 \mu\text{m}$ and then polished with a twin-jet electropolishing machine (Struers TenuPol-5). The hardness of the samples was measured using a Struers DuraScan-70 G5 tester with a load of 10 Kgf for 15 s. Six indentations were measured to obtain the average Vickers hardness. ThermoCalc software (version 2019b with database TCFE 9) was used to predict the equilibrium phase in the alloys.

3. Results

3.1. Microstructure of As-Deposited and Tempered Steels

Figure 2 shows the microstructure of the as-deposited HBS alloy. A fully dense deposited zone was obtained. The optical image clearly shows the melt pools and their boundaries (Figure 2a). The microstructure in the melt pool (the location I in Figure 2a) was different from that at the melt pool boundaries (location II in Figure 2a). In the melt pool (Figure 2I), there are mainly three types of features: 1) the bright phase in a square shape indicated by red arrows, 2) the eutectic regions containing matrix and relatively small bright phase indicated by the blue

arrow, and 3) the dashed regions without any bright phase. The bright phase in HBS was confirmed as M_3B_2 boride by XRD, as shown in Figure 3a. At the melt pool boundaries, M_3B_2 boride was distributed more homogeneously owing to the remelting and solidification. Although relatively dark illumination was observed in those two layers adjacent to the substrate (Figure 2a), no distinct microstructure was revealed (Figure 2III). The dendritic structure has been widely reported in steels fabricated by DED method.^[13–15] However, no such structure was found in the deposited HBS sample.

The microstructure of the as-deposited V4E steel has been reported in our previous work.^[16] Cellular/dendritic structure is the typical microstructure in the as-deposited V4E steel. There are two types of primary carbides in the interdendritic region, i.e., V-enriched MC carbide and Mo- and Cr-enriched M_2C type. Both carbides were also identified by XRD in Figure 3b.

To obtain a high hardness, tempering was applied to the deposited steels. After this heat treatment, the RA in HBS was removed, as seen by XRD in Figure 3a, although no change could be detected in the SEM images (Figure 2 and 4a). Regarding V4E steel, a high fraction of RA was found in the as-deposited sample. In our previous work,^[16] RA was observed in the regions near primary carbides. In the tempered sample, a small amount of RA still existed, as confirmed by the shoulder at the left of the bcc peak in Figure 3b. This was due to the high carbon content (1.4 wt%) in V4E, which led to low M_s and M_f temperature. However, RA was not observed from the SEM image of tempered V4E (Figure 4d); no precipitate was visible neither. The primary carbides, both MC and M_2C carbides, are distributed in the interdendritic regions, as marked in the insert of Figure 4d.

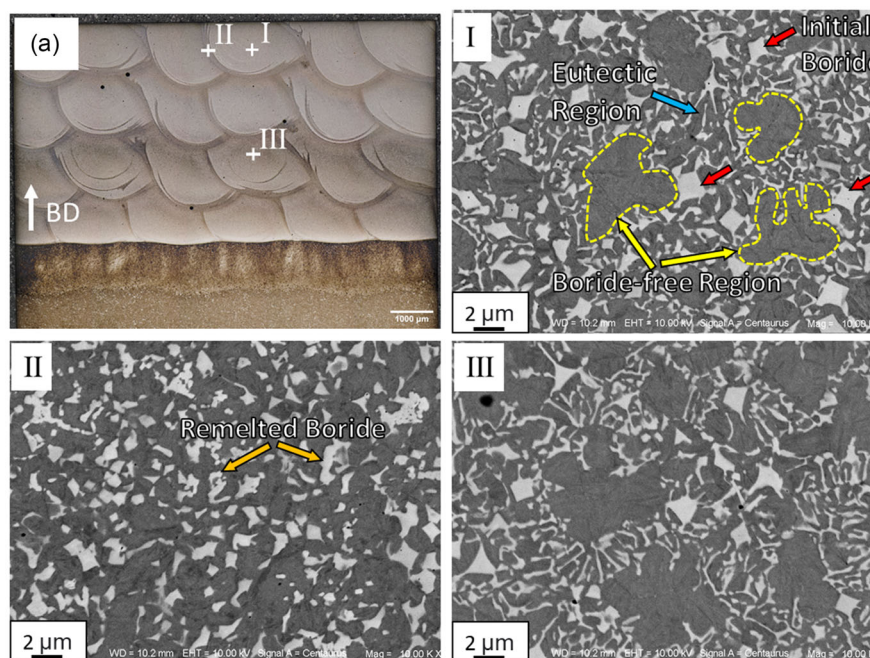


Figure 2. The microstructure of as-deposited HBS alloy: a) optical image from the cross section; I–III) the backscattered scanning electron microscope images from three different locations: (I–III) in (a).

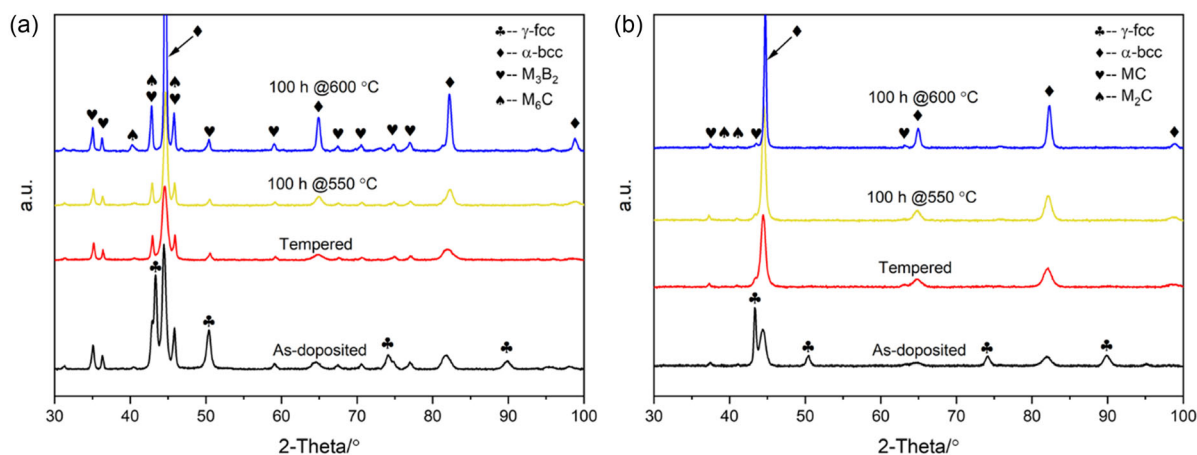


Figure 3. The XRD patterns of two deposited alloys under different conditions: a) HBS and b) V4E.

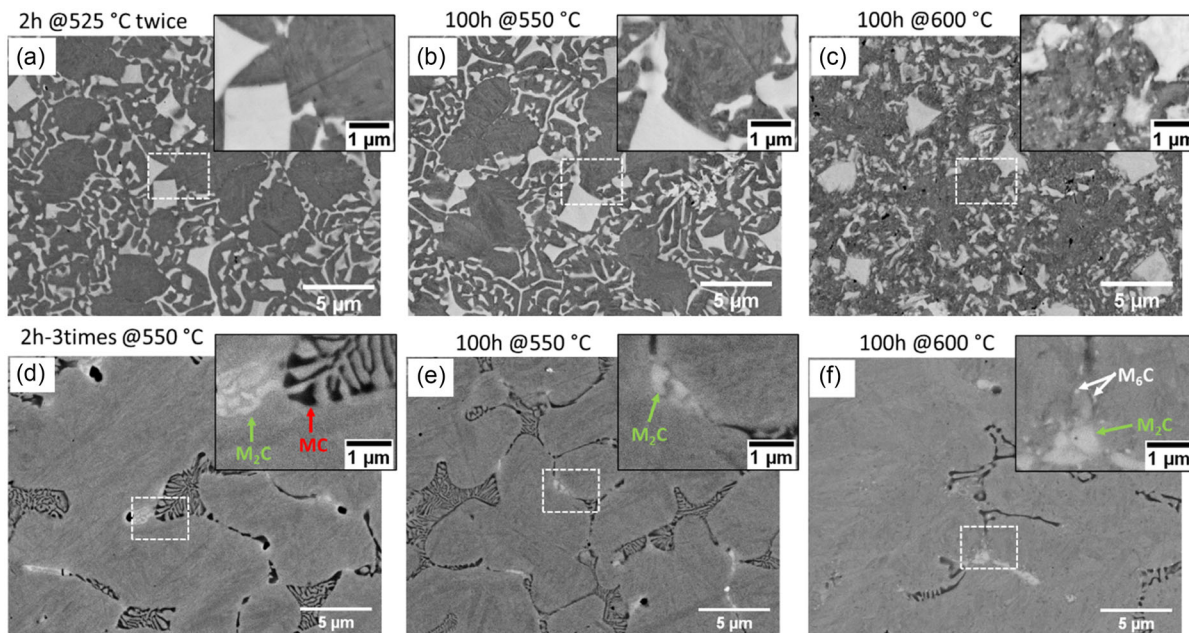


Figure 4. The microstructure evolution before and after softening treatments. HBS alloy at the conditions of a) tempered and softened at b) 550 °C and c) 600 °C. V4E alloy at the conditions of d) tempered and softened at e) 550 °C and f) 600 °C.

3.2. The Softening Behavior at High Temperatures

Figure 5a,b shows the hardness evolution of HBS and V4E steel at high temperatures for different holding times. Tempered HBS alloy obtained a high hardness of 1065 HV. After the softening treatment at 550 °C for 100 h, its hardness was still as high as 906 HV. The reduction of the hardness was just about 159 HV. When increasing the softening temperature to 600 °C, the hardness dropped to 647 HV after 100 h, indicating a significantly higher reduction of 418 HV. As to the V4E steel, it had an overall lower hardness compared with HBS alloy under all conditions (Figure 5b). After the treatment at 550 °C for 100 h, the hardness dropped from 874 HV (tempered condition) to 771 HV, corresponding to a reduction of 103 HV. This is lower than that of

HBS alloy at the same temperature. Increasing the softening temperature to 600 °C, the hardness decreased to 551 HV, meaning a reduction of 323 HV. This is also lower than that of HBS.

The purpose of this investigation was hardfacing. The hardness comparison between the deposited materials and the substrate steel was therefore important. Figure 5c shows the hardness evolutions of the deposited alloys as well as the substrate. As can be seen, the deposited steels had a higher hardness than the substrate steel under all conditions, including the as-deposited, tempered, and softened HBS and V4E at 550 and 600 °C. This suggested that the hardfacing by DED method with the deposited steel grades (HBS and V4E) could be a promising method to improve the wear resistance of hot-forming dies. In addition, the hardness of both materials had a relatively big

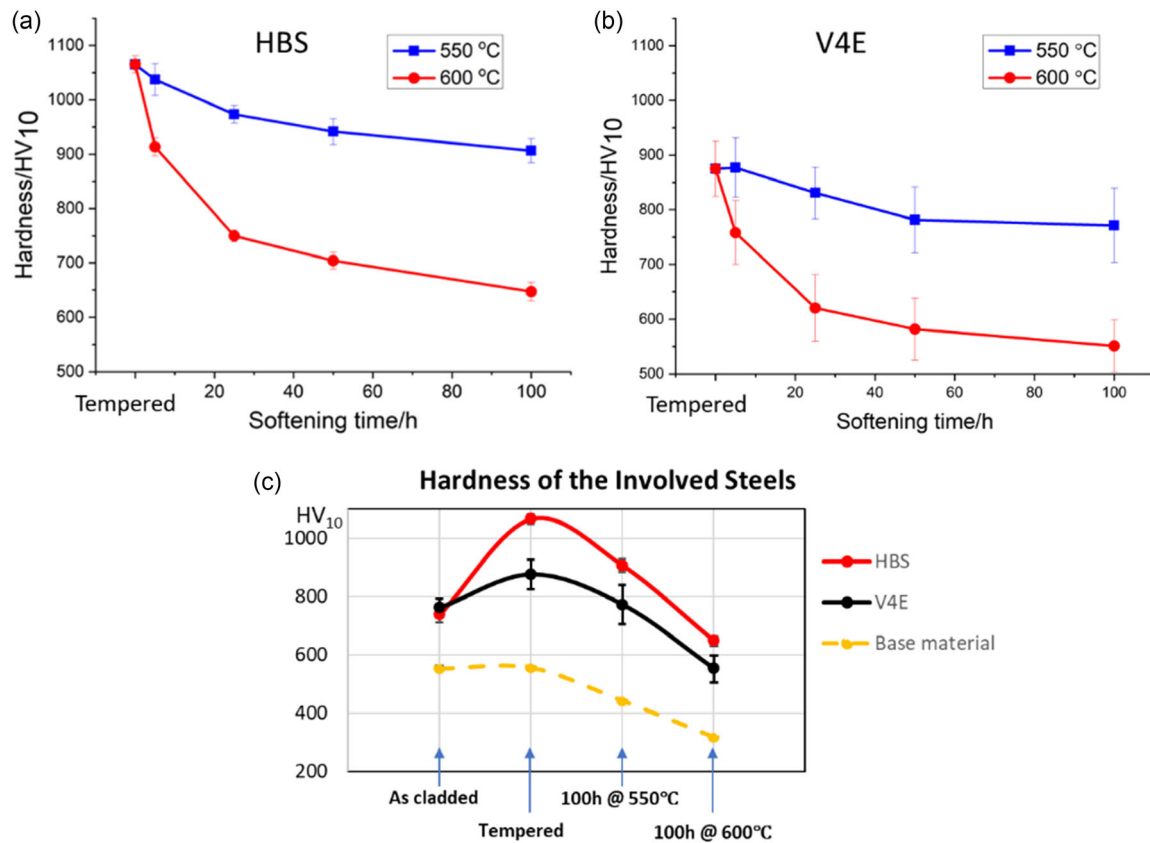


Figure 5. Hardness evolution of the samples as a function of time and temperature a) HBS and b) V4E. c) Comparison between the involved steels at different conditions.

increase from the as-deposited state to the tempered state, attributed to the disappearance of the RA in the materials, which was confirmed by the XRD patterns in Figure 3.

3.3. Microstructure Evolution at High Temperatures

At the as-deposited state, weak M_6C peaks in the XRD patterns of HBS (Figure 3a) indicated a low proportion of this primary carbide obtained from solidification. No obvious change was observed in the sample tempered and softened at 550 °C for 100 h. When the softening temperature was increased to 600 °C, the intensity of M_6C peaks had a distinct increase. Regarding microstructure, no changes could be detected from SEM images in HBS tempered (Figure 4a) and softened at 550 °C for 100 h (Figure 4b). When the softening temperature was increased to 600 °C, some small bright particles precipitated from the matrix, as shown in the insert of Figure 4c. These visible small precipitates were supposed to be M_6C type, as suggested by XRD. In addition to this, the shape of the bright boride phase, as revealed in Figure 2 and 4a,b, became less sharp, presenting a spheroidizing tendency.

To further investigate the microstructure evolution at high temperatures, TEM was applied to inspect the HBS alloy (Figure 6). After double tempering at 525 °C for 2 h, the alloy had a tempered martensite structure with some extremely small

carbides in the matrix (Figure 6a). The relief-like matrix implied a high dislocation density due to the relatively low tempering temperature (525 °C). After the subsequent softening treatment at 550 °C, there were extensive particles precipitated from the matrix (Figure 6b). These particles had a needle-like shape with a narrow width of ≈ 5 nm. It seemed that there was a certain orientation relationship between the matrix and the precipitates. When increasing the softening temperature to 600 °C, the needles were coarsened naturally, and the width increased to ≈ 15 nm. However, XRD was still not able to detect the existence of this precipitate due to its extremely small size. From the unpublished work in our group, these needle-shaped particles are supposed to be the M_7C_3 or $M_{23}C_6$ type carbides. In contrast, some near-square particles could be easily found in the matrix in Figure 6c. They should be the M_6C carbides, which were identified by XRD due to their relatively big size (50–100 nm).

Compared to the tempered condition, the microstructure (SEM images) of V4E did not reveal an obvious difference after the long-term (100 h) softening at 550 °C at the magnification used in this study. For the V4E steel softened at 600 °C for 100 h, some fine white precipitates were observed near the interdendrite region (Figure 4f), which can be easily distinguished from the primary whitish particles (M_2C type) by their morphology. Usually, the whitish particle with a large size (several hundred nanometers) did not change much and is supposed

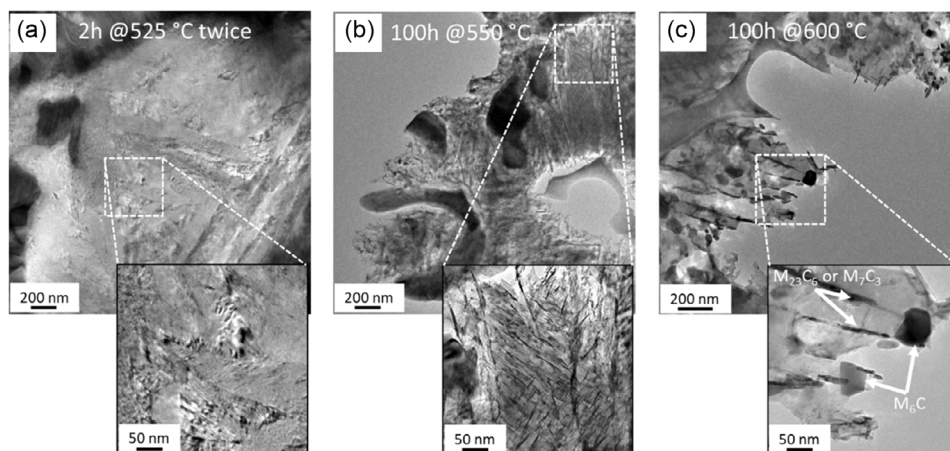


Figure 6. Transmission electron microscopy images from the HBS after a) tempering and b) softening at 550 °C and c) 600 °C for 100 h.

to be the M_2C primary carbides, which has already been identified in ref.[16] and by the XRD pattern in Figure 3b. The small whitish particles cannot be confirmed by XRD due to their extremely low fraction. From the contrast of these newly precipitated particles (Figure 4f), they are suspected to be M_6C carbides enriched with Mo or Cr with high atomic number. The darkish primary carbide is MC type, which was rather stable during the heating. The newly precipitated whitish particles are the secondary carbides with a small size (smaller than 100 nm) and low fraction.

4. Discussion

4.1. Solidification of the As-Deposited Steels

As shown in Figure 2, the microstructure of the as-deposited HBS is unique and contains three types of features: the borides in square shape, the eutectic structure, and the boride-free zone. To explain the formation of this microstructure, prediction of the equilibrium phase in HBS alloy was performed by Thermo-Calc software, as shown in Figure 7a. The first solidified phase in the liquid is the M_3B_2 phase (Stage 1) prior to the solidification of the

γ phase. These initially formed borides are presented as a nearly square shape, indicating a planar growth. With the decrease of temperature (Stage 2), the boride phase and γ phase are solidified simultaneously (Figure 7a), forming the eutectic structure (Figure 8b) that nucleated among dendrites.^[17] Notice that the fraction of the boride M_3B_2 reaches the maximum when Stage 2 is over. Afterward, the remaining liquid will be solidified into the boride-free zone (Figure 2 and 8c). It is seen from Figure 7a that the solidification temperature ranges of the boride and matrix (γ phase) are close, implying that there is little room for the formation of the boride-free zone after Stages 1 and 2. However, considering the fast-cooling rate of DED, more iron-enriched liquid will be preserved to a lower temperature at which little boron was left. Hence, the liquid with a big supercooling degree will transform into the matrix without the boride (Figure 8c).

The solidification of V4E steel is different from that of HBS alloy. As shown in Figure 7b, the phase that solidified first in V4E liquid was the γ phase, which formed a dendritic structure. In the last stage of solidification, the MC phase is formed and solidified simultaneously with the γ matrix. This can explain the formation of the eutectic structure located at the interdendritic region

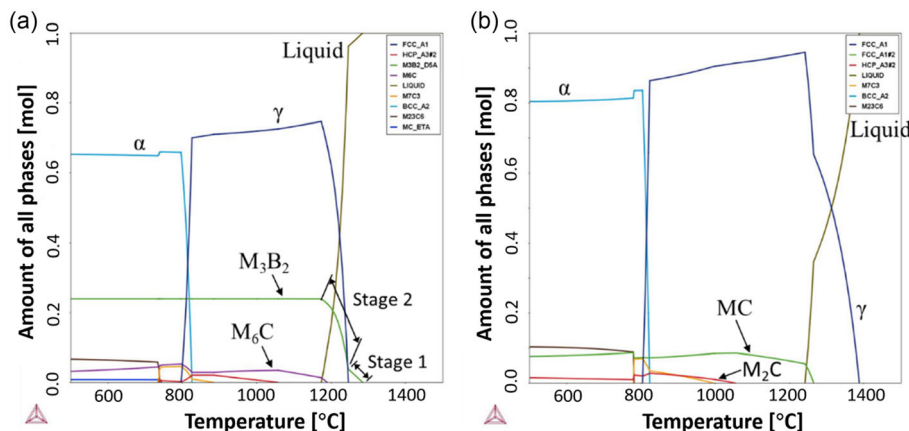


Figure 7. Prediction of the equilibrium phase by Thermo-Calc thermodynamic calculations for a) HBS and b) V4E.

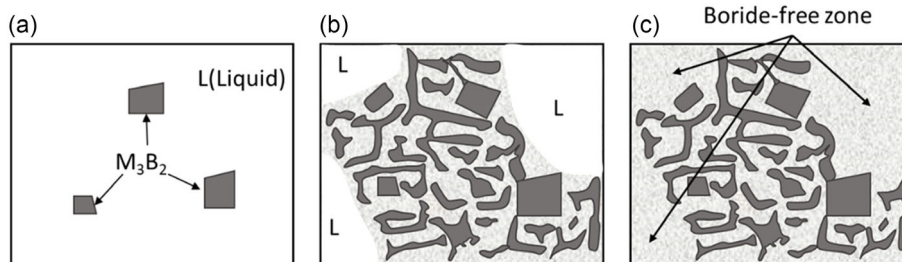


Figure 8. Schematic diagram for the solidification process of HBS alloy. a,b) Stage 1 and stage 2 in Figure 7a. c) Solidification is completed.

(Figure 4). However, some M_2C particles are found in the as-deposited materials.^[16] The formation of this phase is probably attributed to the redistribution of the solutes in liquid and the big supercooling degree caused by the fast cooling. The low-temperature liquid at the last stage of solidification leads to the formation of M_2C carbides as one of the primary carbides in V4E.

4.2. Softening Mechanism

In general, the hardness of steels exhibits a linear relationship with the strength. It is determined by many factors, such as precipitation hardening, dislocation density, grain size, and so on. The changes in the hardness of steels can be discussed by evaluating these factors. For HBS alloy, the hardness increases significantly after tempering (Figure 5c). This is mainly attributed to the removal of the RA phase in the as-deposited sample (Figure 3a). The peak hardness of HBS reaches 1065 HV after tempering, which is higher than most of hot work tool steels. A large amount of hard phase (M_3B_2) is one of the key reasons for the high hardness. From the report of Tomota et al.,^[18] the hardness of the M_3B_2 boride is in a range of 1600–2400 HV. Considering the high fraction of this primary hard phase, the conceptual design of this alloy exhibits some similarities to cemented carbides. Borides act as the primary hard phase and the iron-based material is a binder. Another reason for the high hardness is the hard matrix with tempered martensite. As can be seen in Figure 6a, even with the double tempering at 525 °C for 2 h, the matrix still reveals a relief-like structure, implying a high dislocation density in the material. Momotani et al.^[19] investigated an interstitial free steel and found that the dislocation density of the steel does not change much and remains at a high level ($>10^{14} \text{ m}^{-2}$) after high-temperature tempering. This implied that the steel has the potential to retain a high density of dislocations at high temperatures if there is no carbide precipitation to consume dislocation energy. In the present study, carbides are rarely found in the tempered HBS samples, which also supports this argument. In contrast, far more precipitates in Figure 6b imply a supersaturated solid solution in the tempered condition. In this case, solid solution strengthening by alloying elements should be a factor that cannot be ignored. During the subsequent softening at 550 °C, the hardness of the HBS alloy decreases gradually with time (Figure 5b). As revealed by the TEM images in Figure 6b, the major change at this temperature is the extensive precipitation in the matrix. The precipitate in a needlelike shape has a width of about 5 nm. It seems that there exists an

orientation relationship between the precipitates and the matrix. The extremely small size is probably the reason that this phase cannot be detected by XRD. Although the precipitates could contribute to the strengthening, there is competition among dislocation strengthening, solid solution strengthening, and precipitation strengthening. After the thermal treatment, the precipitation strengthening effect increases, but the dislocation strengthening and solid solution strengthening effects are weakened, leading to a decrease in final hardness, as exhibited in Figure 5a. When increasing the softening temperature to 600 °C, the hardness of HBS alloy has a further decrease compared to that at 550 °C. The coarsening of the precipitates (Figure 6c) and the lowered dislocation density are the reasons. Usually, the primary hard boride M_3B_2 is rather stable in both volume fraction and size during softening treatments and will have little influence on the change of hardness.

Compared to HBS alloy, V4E reveals a similar softening tendency at high temperatures of 550 and 600 °C. However, V4E steel shows a better softening resistance than HBS, as mentioned in Section 3.2. TEM is supposed to be a suitable technique to characterize the microstructure evolution of V4E steel. Due to the defects in this steel, unfortunately, TEM samples were not able to be prepared successfully at this stage. However, some conclusions can still be drawn when compared with HBS. The high dislocation density in the tempered HBS is due to the relatively low tempering temperature (525 °C). Notice V4E steel was tempered at 550 °C, which is equal to one of the subsequent softening temperatures. The dislocations could be eliminated more during tempering and their density will not have a significant decrease during the softening stage. As stated by many other researchers,^[20–22] dislocation density often decreases dramatically at the beginning of high-temperature tempering, and then tends to be relatively stable. Another factor that may influence the softening resistance is the precipitates in V4E. In another work (not published yet) of this group, massive dark precipitates are observed in the V4E sample softened at 800 °C for 3 h. They are identified as V-enriched MC. Considering MC carbide is a thermal stable carbide for V4E, as indicated by the simulation results in Figure 7b, it is reasonable to assume that treating at 800 °C for 3 h is an accelerated version of 600 °C for 100 h. This type of carbide is more stable than Cr-enriched $M_{23}C_6$ or M_7C_3 in HBS. Thermodynamic calculation^[23] indicates that MC carbide has a much lower interfacial energy and higher thermodynamic driving force than other carbides (e.g., M_7C_3 , $M_{23}C_6$, M_6C , M_3C) in Fe-based materials. This leads to a much smaller nucleation barrier and critical radius for MC precipitation.

Meanwhile, the coarsening tendency is small. Hence, nanoscale MC precipitates can be formed in the tempered V4E steel. The tiny MC carbide is supposed to be massively formed in the V4E sample at 600 °C for 100 h as well. This should be one of the reasons for the better softening resistance of V4E. The extremely small size makes it difficult to be observed by SEM. In contrast, the V-enriched MC carbide in V4E steel is a very hard phase. This could be another reason that V4E shows a better softening resistance. Although M_6C particles are found in the microstructure formed at 600 °C for 100 h, most of them are distributed within the eutectic region. This indicates that only the matrix solidified at the final stage (high alloying element content) is able to precipitate visible M_6C carbides. This type of carbide may provide some hardening effect. However, considering that M_6C also exists in HBS alloy, the contribution of this carbide to the softening resistance of V4E is expected to be limited.

5. Conclusion

The present study addresses a critical concern in the automotive industry, i.e., extension of the lifetime of hot stamping dies by additive manufacturing. Two specific types of tool steels namely V4E and HBS were deposited on a tool steel substrate through a DED process, followed by tempering. The softening resistance of the steels at high temperatures has been assessed. The microstructures and their correlation to hardness have been discussed. The findings of this investigation are summarized as follows: 1) two steels investigated exhibited a remarkable increase in hardness in both as-deposited and as-tempered conditions compared to that of the underlying substrate tool steel. For HBS alloy, an ultrahigh hardness of 1065 HV is obtained after tempering. When subjecting to exposure at 550 and 600 °C for 100 h, the hardness of these two steels is still higher than that of the substrate under the same conditions, implying that DED is a promising method for hardfacing hot stamping die to improve the mechanical properties and to extend the tool life. 2) HBS alloy obtained a fully dense structure. A typical microstructure of as-deposited HBS consists of primary borides, eutectic regions, and boride-free regions. In contrast, as-deposited V4E presents a dendritic structure with primary carbides in the interdendritic region. RA existed in as-deposited condition was removed by tempering for both steels. 3) HBS steel demonstrated exceptional resistance to softening at 550 °C, with only a minor reduction in hardness. However, at 600 °C, a substantial decrease in hardness became evident. V4E, in contrast, displayed superior overall resistance to softening, experiencing smaller decreases in hardness at both 550 and 600 °C compared to HBS. 4) The changes in hardness in these steels were attributed to various factors, including the elimination of RA, the development of hard phases, variations in dislocation density, and strengthening through solid solution. For HBS alloy, the decrease of dislocation density and loss of solid solution strengthening are the major reasons for softening at 550 °C. Coarsening of precipitates contributes to further softening at 600 °C. For V4E steel, more stable dislocation density and the presence of thermally stable carbides (V-enriched MC carbides) contribute to better softening resistance than HBS alloy.

The findings in this study illuminate the complex relationship between microstructure, hardness characteristics, and softening behavior of these materials when exposed to high temperatures. The results provide some valuable insights that can guide further exploration and practical applications in related fields including the automotive industry.

Acknowledgements

This study is supported by Production Area of Advance, Chalmers University of Technology, China Scholarship Council (grant no. 201806370253), Uddeholms AB, Sweden, and ASSAB Tooling Technology, China.

Conflict of Interest

The authors declare no conflict of interest.

Data Availability Statement

The data that support the findings of this study are available from the corresponding author upon reasonable request.

Keywords

borides, carbides, directed energy deposition, hot stamping, softening resistance, tool steels

Received: March 27, 2023

Revised: October 9, 2023

Published online:

- [1] ASTM Standard, *Standard Terminology for Additive Manufacturing Technologies*, ASTM Int. F2792–12a, West Conshohocken **2012**.
- [2] L. Gibson, D. Rosen, B. Stucker, M. Khorasani, *Additive Manufacturing Technologies*, Springer, Cham **2021**, p. 23.
- [3] S. H. Wang, J. Y. Chen, L. Xue, *Surf. Coat. Technol.* **2006**, 200, 3446.
- [4] P. Kattire, S. Paul, R. Singh, W. Yan, *J. Manuf. Processes* **2015**, 20, 492.
- [5] B. D. Beake, L. Ning, C. Gey, S. C. Veldhuis, A. B. Kornberg, A. Weaver, M. Khanna, G. S. Fox-Rabinovich, *Surf. Coat. Technol.* **2015**, 279, 118.
- [6] M. Pellizzari, *Wear* **2011**, 271, 2089.
- [7] C. Boher, S. L. Roux, L. Penazzi, C. Dessain, *Wear* **2012**, 294, 286.
- [8] C. Y. Chou, N. H. Pettersson, A. Durga, F. Zhang, C. Oikonomou, A. Borgenstam, J. Odqvist, G. Lindwall, *Acta Mater.* **2021**, 215, 117044.
- [9] G. W. Park, S. Shin, J. Y. Kim, Y. M. Koo, W. Lee, K. A. Lee, S. S. Park, J. B. Jeon, *J. Alloys Compd.* **2022**, 907, 164523.
- [10] J. S. Park, J. H. Park, M. G. Lee, J. H. Sung, K. J. Cha, D. H. Kim, *Mater. Trans. A* **2016**, 47, 2529.
- [11] N. U. Rahman, L. Capuano, S. Cabeza, M. Feinaeugle, A. Garcia-Junceda, M. B. De Rooij, D. T. A. Matthews, G. Walmag, I. Gibson, G. R. B. E. Römer, *Addit. Manuf.* **2019**, 30, 100838.
- [12] Y. Eun Jeong, G. Y. Shin, D. S. Shim, *J. Manuf. Processes* **2021**, 68, 1596.
- [13] G. Telasang, J. D. Majumdar, G. Padmanabham, M. Tak, I. Manna, *Surf. Coat. Technol.* **2014**, 258, 1108.

- [14] J. Choi, Y. Chang, *Int. J. Mach. Tools Manuf.* **2005**, 45, 597.
- [15] P. Bajaj, A. Hariharan, A. Kini, P. Kürnsteiner, D. Raabe, E. A. Jägle, *Mater. Sci. Eng., A* **2020**, 772, 138633.
- [16] M. Yuan, S. Karamchedu, Y. Fan, L. Liu, L. Nyborg, Y. Cao, *J. Manuf. Processes* **2022**, 76, 419.
- [17] K. Y. Luo, X. Xu, Z. Zhao, S. S. Zhao, Z. G. Cheng, J. Z. Lu, *J. Mater. Process. Technol.* **2019**, 263, 50.
- [18] Y. Tomota, K. Kuroki, T. Mori, I. Tamura, *Mater. Sci. Eng.* **1976**, 24, 85.
- [19] Y. Momotani, A. Shibata, T. Yonemura, Y. Bai, N. Tsuji, *Scr. Mater.* **2020**, 178, 318.
- [20] T. Zhou, J. Faleskog, R. P. Babu, J. Odqvist, H. Yu, P. Hedström, *Mater. Sci. Eng., A* **2019**, 745, 420.
- [21] J. Sjöström, *PhD Thesis, Karlstad University* **2004**.
- [22] N. Du, H. Liu, P. Fu, H. Liu, C. Sun, Y. Cao, D. Li, *Crystals* **2020**, 10, 238.
- [23] T. Zhou, R. P. Babu, Z. Hou, J. Odqvist, P. Hedström, *Materialia* **2020**, 9, 100630.